Ceramics International 45 (2019) 21843–21850

Contents lists available at ScienceDirect

Ceramics International

journal homepage: www.elsevier.com/locate/ceramint

Layered extrusion forming of complex ceramic structures using starch as removable support

Li Yang, Shiyan Tang, Guanjin Li, Lei Qian, Jinkai Mei, Wenming Jiang, Zitian Fan*

State Key Laboratory of Materials Processing and Die & Mould Technology, Huazhong University of Science and Technology, Wuhan, 430074, Hubei, China

ARTICLE INFO

Keywords:
Additive manufacturing
Layered extrusion forming
Support material
Starch
Ceramic parts

ABSTRACT

This paper presents a sustainable starch-based slurry that can be used as support material for the 3D printing of complex ceramic parts. The slurry was first prepared by using starch, polyvinylpyrrolidone (PVP), and absolute ethyl alcohol. The rheological properties of the starch-based slurry with different solid loadings, as well as the dimensional deviation rate and bending strength of the green body after drying, were studied. A grid sample was printed to verify its support feasibility, and thermogravimetric analysis was performed to determine the burn loss of the starch-based support material. The results showed that the prepared starch slurry possessed desired rheological and support properties. The size deviation rate of the printed sample was approximately 1.1% after drying, and the bending strength was sufficient (> 11 MPa). Additionally, the drying speed of the slurry was fast, the preparation process simple, and the cost low. The starch support could be completely burned away at 500 °C without residue or reacting with the matrix material. The development of this slurry will significantly promote the rapid preparation of complex ceramic components, thereby extending the possibility for a wider application of 3D printing technology in ceramics.

1. Introduction

Owing to their various excellent properties, ceramics are used in a wide range of applications, including the chemical industry, machinery, electronics, aerospace, biomedical engineering, and casting. Traditional ceramic preparation processes mainly include injection molding, tape casting, and gel casting [1–5]. However, these ceramic forming techniques are limited in terms of long processing times, high cost, and mold compatibility. With the rapid development of science and technology, specially shaped ceramic components with complex structures have become increasingly popular, but cannot be formed with molds, which greatly limits the design possibilities. In recent years, rapidly evolving 3D printing technology has provided a new solution for this purpose [6]. 3D printing technology can produce very complex and precise structures with a unique manufacturing concept. According to domestic and foreign research reports, the 3D printing technologies that can be used to prepare ceramic components primarily include 3DP [7], ink jet printing [8,9], stereolithography [10,11], selective laser sintering [12], and direct ink writing [13–17]. Direct ink writing—also known as robocasting (RC) and layered extrusion forming (LEF)—was first filed as a patent by Cesarano and co-workers at Sandia National Laboratories in 1997 [18]. In LEF, a viscoelastic slurry is extruded through a fine nozzle, and the layers are stacked to form a designed shape. Compared with other additive manufacturing methods, LEF possesses the advantages of low equipment and material costs, simple process, good environmental adaptability, and an adjustable production rate by way of changing the nozzle diameter [19]. According to the literature, LEF is mostly used to prepare biological scaffolds, piezoelectric ceramics, food, etc. [20–22]. However, the structure of the parts prepared by LEF is relatively simple at present. To prepare complex components, it is necessary to print additional structural objects to support the product geometry, and those supports must be removed from the geometry easily. Double-head extrusion was proposed to print two materials in a two-dimensional plane—one to form the main part and the other to form the support structure [23].

The slurry used as a support material must meet the typical requirements of the LEF equipment—that is, it must maintain its shape under the overburden and flow smoothly from the fine nozzle under high shear stress. Additionally, the support material should be chemically compatible with the main material and easily removed during post-treatment without any additional products. Currently, the materials used for supports are mainly calcium-carbonate- and graphite-based. Calcium carbonate will turn into calcium oxide after sintering, which is easily removed by reacting with water and acid [24,25]. Graphite will burn away at 800 °C after drying without residues. However, the solid loading of graphite slurry is less than 50 wt.% and

* Corresponding author.
E-mail address: fanzt@hust.edu.cn (Z. Fan).

https://doi.org/10.1016/j.ceramint.2019.07.193
Received 31 May 2019; Received in revised form 15 July 2019; Accepted 16 July 2019
Available online 17 July 2019

the bending strength is only 1.04 ± 0.04 MPa after drying [26]. This low solid loading and bending strength will lead to a high size deviation rate after drying and cracking in the stacking process, respectively. Therefore, it is necessary to find a support material with high solid loading (thereby reducing the drying size deviation rate) and high bending strength that can be burned away in the sintering process.

In this paper, a method for preparing complex ceramics by LEF using starch as a support is presented. Starch is an inexpensive, readily available material, non-toxic material. Furthermore, it does not pollute the environment after burning. Herein, slurry is first prepared using starch, polyvinylpyrrolidone (PVP), and absolute ethyl alcohol. Subsequently, the properties of the starch-based slurry and printed sample are tested. Finally, a complex ceramic component blank is prepared by a double-head LEF device, and a desired ceramic part was obtained after drying, degreasing, and sintering.

2. Experimental procedure

2.1. Raw materials

Starch (≥99.5 wt.% purity; D_{50} = 29.50 μm Sinopharm Chemical Reagent Co., Ltd., China) was used as the raw material of the support without further treatment. Fig. 1(a) shows the starch particle size distribution. The chemical composition of the starch powder was $(C_6H_{10}O_5)_n$. And the main parameters of the starch are listed in Table 1. PVP (≥99.5 wt.% purity; Qingdao Usolf Chemical Technology Co., Ltd., China) was used as an organic binder and rheology modifier to promote uniform dispersion of the slurry by improving the steric hindrance of the starch particles. Anhydrous ethanol (EtOH, ≥99.5 wt.% purity; Sinopharm Chemical Reagent Co., Ltd., China) was used as the solvent of the slurry. Methyl silicone oil was applied to the printing substrate so that the printed samples could be separated from the substrate easily. The concentration of PVP binder was 15% in weight. Table 2 shows the mass fraction of each component in the different slurries.

It was necessary to prepare an alumina ceramic slurry for printing complex alumina ceramic parts to test the support effect of the optimized starch-based slurry. The Al_2O_3 slurry was prepared from Al_2O_3 powder (≥98.5 wt.% purity; D_{50} = 7.77 μm; Qingdao Almatis Co., Ltd., China). The particle size distribution of the Al_2O_3 powder is shown in Fig. 1(b). A 10% PVP (≥99.5 wt.% purity; Qingdao Usolf Chemical Technology Co., Ltd., China) deionized solution was used as an organic binder and rheology modifier. Acetic acid (≥99.5 wt.% purity, Sinopharm Chemical Reagent Co., Ltd., China) and Octanol (≥99.5 wt.% purity; Sinopharm Chemical Reagent Co., Ltd., China) were used as the dispersant and defoaming agent, respectively.

Table 1
Main parameters of starch.

Chemical formula	Purity	Residue on ignition	pH (20 g/L, 25 °C)
$(C_6H_{10}O_5)_n$	≥99.5 wt.%	≤0.5% wt.%	6.0–7.5

Table 2
Components of starch slurries.

Items	Starch (wt.%)	PVP (wt.%)	EtOH (wt.%)
1	71.4	4.3	24.3
2	73.3	4	22.7
3	75	3.7	21.3

2.2. Robocasting

A self-developed double extrusion head printing device was used in this work, which included a drive mechanism, control mechanism, and motion mechanism. A syringe could move along the x and z axes to deposit the slurry in a layer-wise pattern on the substrate. A host computer was employed to translate a 3D model into a path file that controlled the path of the syringe. A pneumatic controller provided pressurized air as the driving force for the extrusion of the slurry.

First, we needed to test the printing effectiveness of the starch slurry. The detailed nozzle diameter, layer height, and printing speed values are listed in Table 3.

Fig. 2 shows a schematic diagram of the complex ceramic component forming process. As shown in Fig. 2, the complex ceramic preparation process can be divided into four steps: slurry preparation, printing, drying, and sintering. First, two kinds of slurries (starch slurry and ceramic slurry) were prepared and loaded into syringes after setting the printing parameters. Second, the two slurries were printed on a two-dimensional plane—each layer was extruded onto the previous layer in the z-axis direction. This process was repeated until the desired structure was formed. Subsequently, the green bodies were placed in a drying oven at 50 °C for 10 h. Finally, the dried samples were sintered in a sintering furnace in air, during which the starch was burned away, and the ceramic sample was obtained after cooling to room temperature.

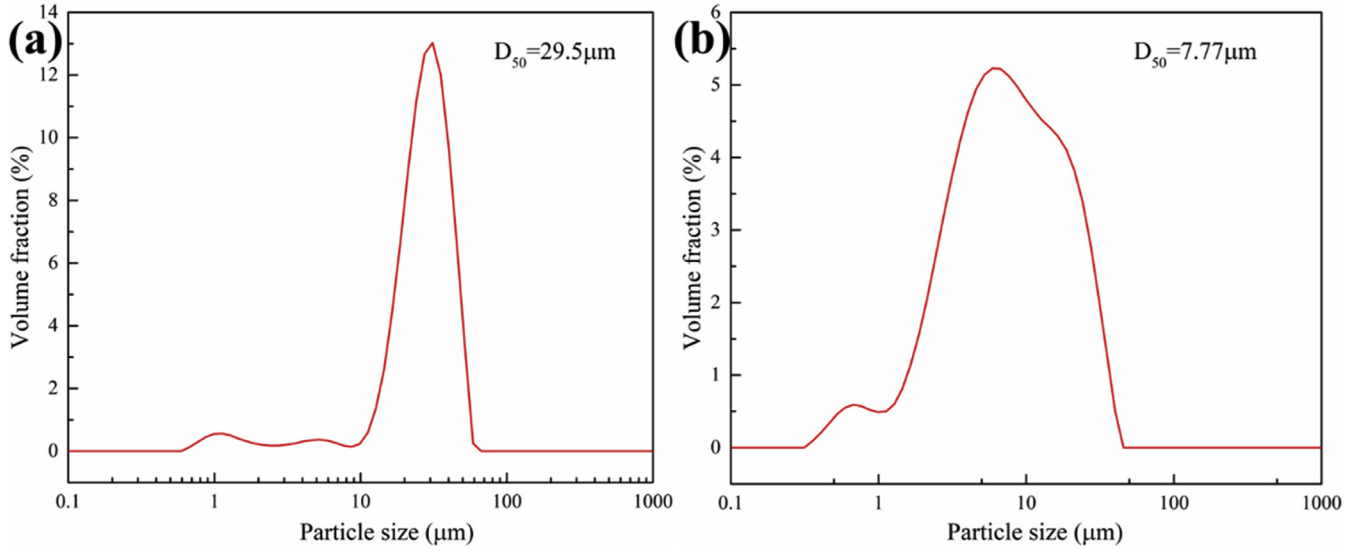

Fig. 1. Particle size distribution of (a) starch and (b) Al_2O_3.

Table 3
LEF printing parameters for starch slurry.

Printing parameters	Values
Nozzle diameter	0.41 mm
Layer height	0.4 mm
Printing speed	20 mm/s

2.3. Characterizations

The particle size distribution was measured with a laser size detector (MS3000, Malvern Instruments, UK). The rheological behaviors were evaluated using a stress-controlled rheometer (DHR-2, TA, USA) with a parallel plate of 25 mm in diameter and testing gap of 1000 μm. Thermogravimetric analysis (Diamond TG/TGA, PerkinElmer Instruments) of the green starch body was conducted after drying. The data was measured in air and heated from room temperature to 800 °C at a heating rate of 10 °C/min. The three-point (3P) bending strength of four starch samples was measured with an ElectroPuls all-electric dynamic fatigue testing system (ElectroPuls E1000, Instron, USA) [27]. The 3P bending strength test was performed under the working parameters of 40 mm span and 0.5 mm/min loading rate. The microstructures of the starch specimens were observed by scanning electron microscopy (Quanta200, FEI, the Netherlands). An optical microscope (Stemi 508, Carl Zeiss) was used to observe the loading of the mesh structure.

The size deviation rate of four starch samples after drying was calculated according to dimensional measurements with Eq. (1):

$$k = \frac{l_2 - l_1}{l_1} \tag{1}$$

Where k is the size deviation rate, l_1 is the original design length, and l_2 is the length after drying. The design size of the sample is 64 × 16 × 4 mm in length, width, and height, respectively.

3. Results and discussion

First, the rheological properties of the starch-based slurry were tested to determine whether they met the requirements of the extrusion process. The rheology of the slurry is crucial for both the LEF process and the fabrication of geometries [28]. Fig. 3 depicts the viscosity versus the shear rate for the different starch solid loadings.

As shown in Fig. 3, the viscosity decreased as the shear rate increased, and the slurry showed a shear-thinning behavior. Shear-thinning behavior enables the slurries to be extruded smoothly through the nozzle and the extruded filaments would rapidly solidify in the absence of shear force [29–31]. The shear thinning flow characteristics indicated that the particles aggregated in the slurries were broken down into smaller flow units by the applied forces, such that the resistance to flow was reduced, leading to a lower viscosity as the shear rate increased. This dependence between the viscosity and shear rate can be described by the power-law model, as shown in Eq. (2) [32]:

$$\eta = K\dot{\gamma}^{n-1} \tag{2}$$

where η is the viscosity, K is the consistency index, $\dot{\gamma}$ is the shear rate, and n is the flow behavior index.

As shown in Table 4, after preliminary fitting and calculating, the values of the exponent $0 < n < 1$ for the slurries clearly show their shear thinning behavior, which is the forceful evidence of the shear-thinning behavior [33]. Additionally, when the shear rate was constant, the viscosity of the slurry increased with the starch solid loading.

According to Table 4, starch slurries containing 71.4 wt.% to 75 wt.% solid loading exhibited shear-thinning behavior and were theoretically suitable for LEF, thus cuboid specimens were printed to verify the printing quality. Fig. 4 shows the surface morphology of the cubic samples of different starch solid loadings. As shown in Fig. 4 (a) and (b), when the starch solid loading was 71.4 wt.% and 73.3 wt.%, the surface of the sample was smooth. However, according to our practical experiments, when the solid loading of the slurry was ≤71.4 wt.%, the printing process was prone to collapse because of slow curing and the size deviation rate of the samples was large after drying. For the slurry containing 73.3 wt.% starch loading, the extrusion process was smooth and without clogging, and no collapse occurred during the formation process.

As shown in Fig. 4 (c) and (d), as the starch solid loading was 75 wt.%, the surface of the sample was rough, and the needle would be clogged occasionally, resulting in the surface flaws. The reasonable explanation is that the solid loading of slurry is high, which leads to a relatively high curing speed. Therefore, slurry with solid loading ≥75 wt.% is not suitable for printing, especially as a support for complex structures.

Fig. 5 illustrates the size deviation rate of the samples compared to the original design size for the different starch solid loadings. As shown in Fig. 5, the size deviation rate of the samples decreased as the starch solid loading increased. The reason for this is that high solid loading results in a low size deviation rate after drying.

Fig. 6 shows the bending strengths of the cuboid specimens with different starch solid loadings after drying. As shown in Fig. 6, the dry bending strengths of the samples with different solid loadings generally exceed 11 MPa.

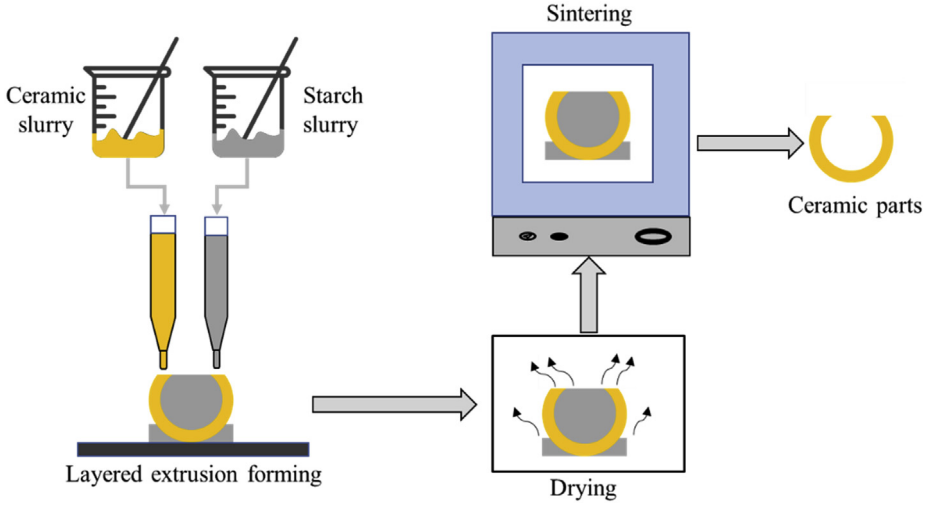

Fig. 2. Schematic diagram of the complex ceramic component forming process.

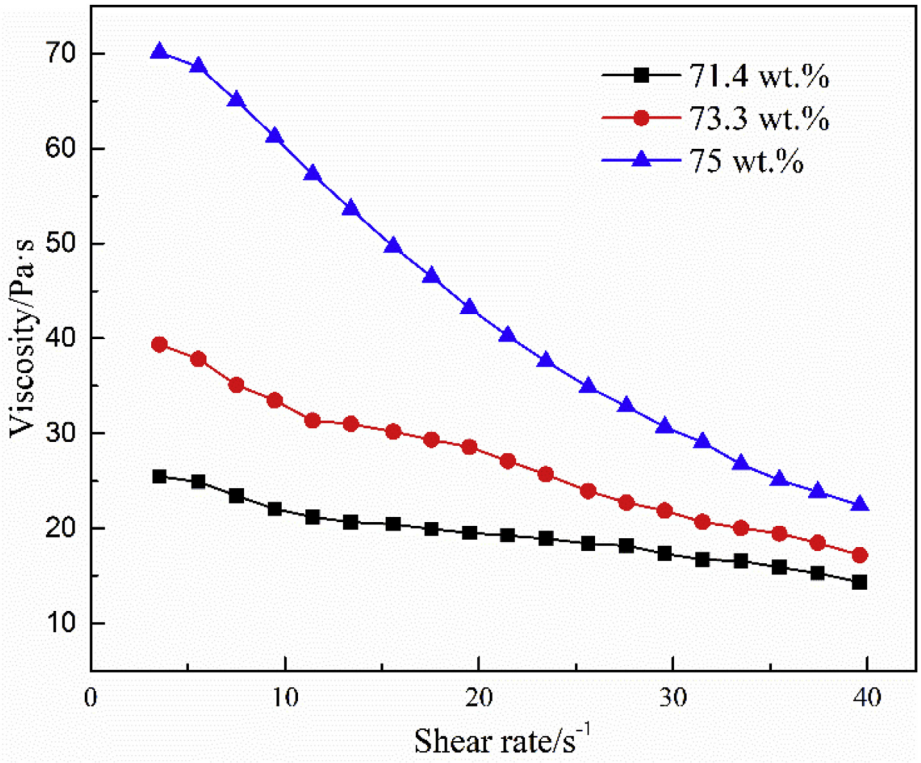

Fig. 3. Viscosity versus shear rate of slurries containing different starch solid loadings.

Table 4
Fitting parameters of slurries containing different starch solid loadings.

Solid loading (wt.%)	K (Pa·s^n)	n	R^2
71.4	35.08	0.79	0.93
73.3	63.31	0.70	0.90
75	139.14	0.58	0.88

Besides the printing quality, another significant characteristic for the support material is constructing the suspended structure without collapse of the final 3D lattices. To examine the ability to withstand the load during formation and the support effect, starch samples with scaffold structures were prepared. As shown in Fig. 7, when the solid loading was 71.4 wt.%, the surface was equipped with smaller pores and swelled starch filaments, and the fracture presented evident collapse as the starch filaments connected with each other and the

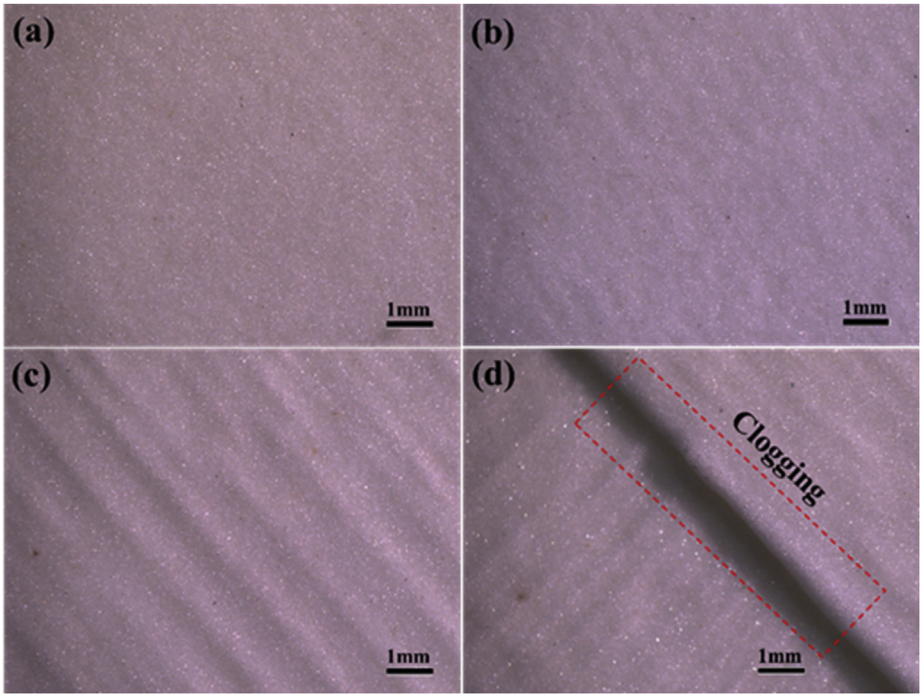

Fig. 4. Surface morphology of samples of different starch solid loadings: (a) 71.4 wt.%; (b) 73.3 wt.%; (c), (d) 75 wt.%.

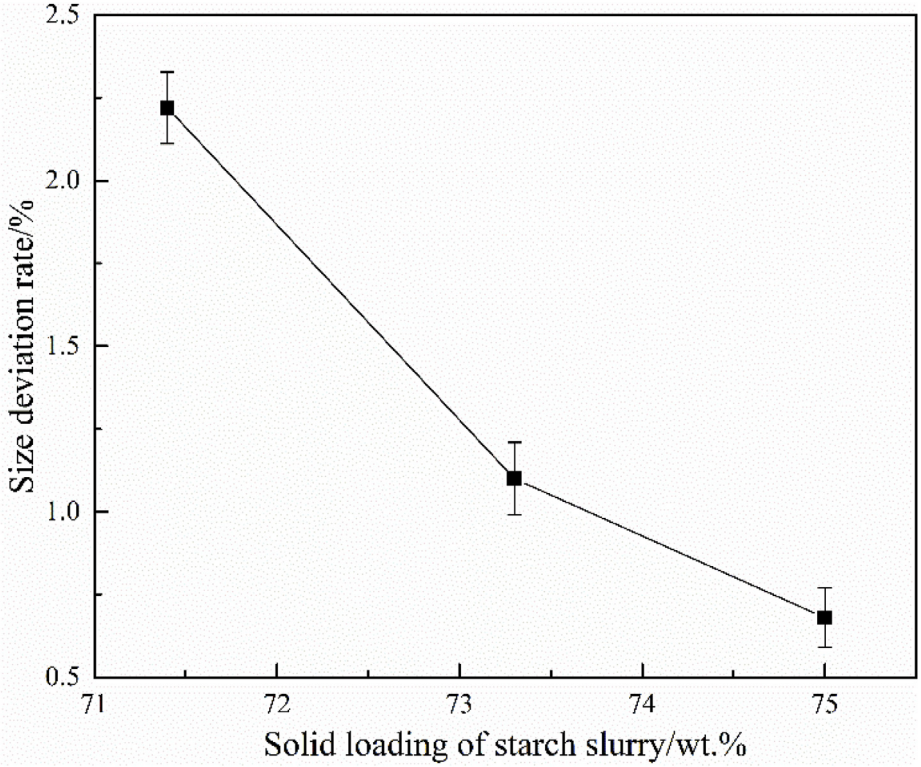

Fig. 5. Size deviation rate of samples with different starch solid loadings after drying.

theoretically existing grids structure was squeezed.

As shown in Fig. 8, when the starch loading was 73.3 wt.%, the scaffold was uniform without distortion. The printed rod cross section exposed a definite circular arrangement and did not become elliptical under weight of the covering material. When a gap was crossed, the printed rod stayed straight and did not sag into a catenary shape. The span was evidently larger than the rod diameter, as shown in Fig. 8(b), and there was no visible collapse or deformation, which is conducive to the integrity of the support. If the support material had collapsed and deformed to varying degrees during the printing process, the main

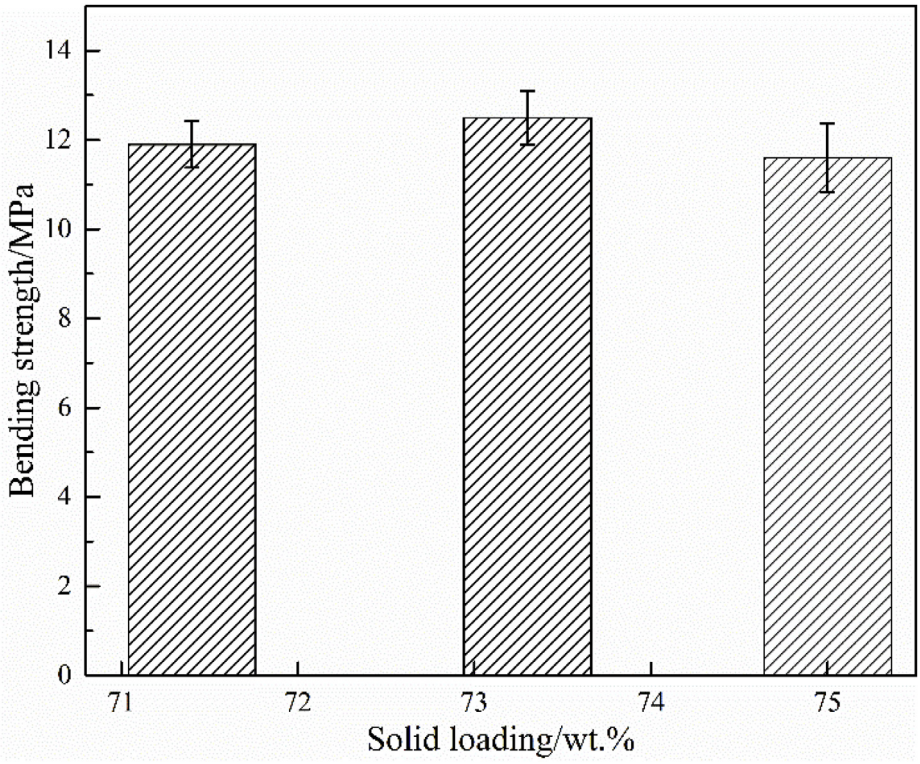

Fig. 6. Bending strengths of samples with different starch solid loadings after drying.

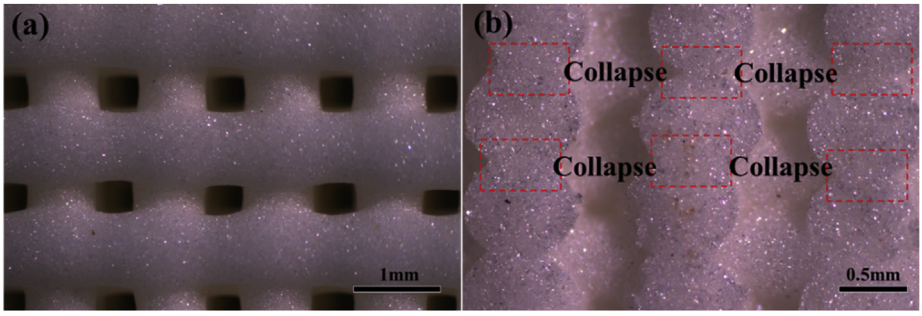

Fig. 7. Optical microscopic image of scaffold with a solid loading of 71.4 wt.%: (a) surface; (b) fracture.

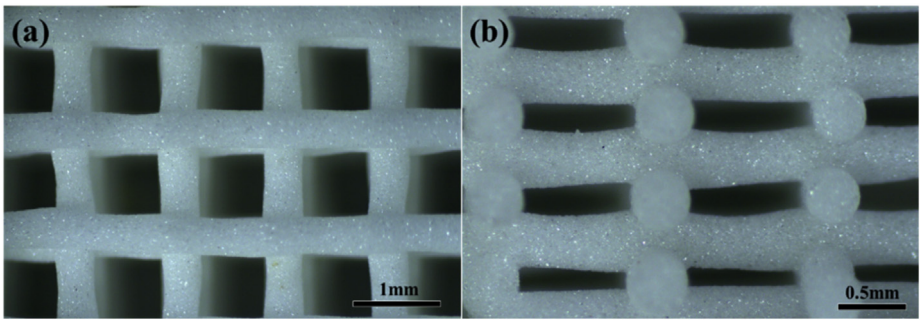

Fig. 8. Optical microscopic image of scaffold with a solid loading of 73.3 wt.%: (a) surface; (b) fracture.

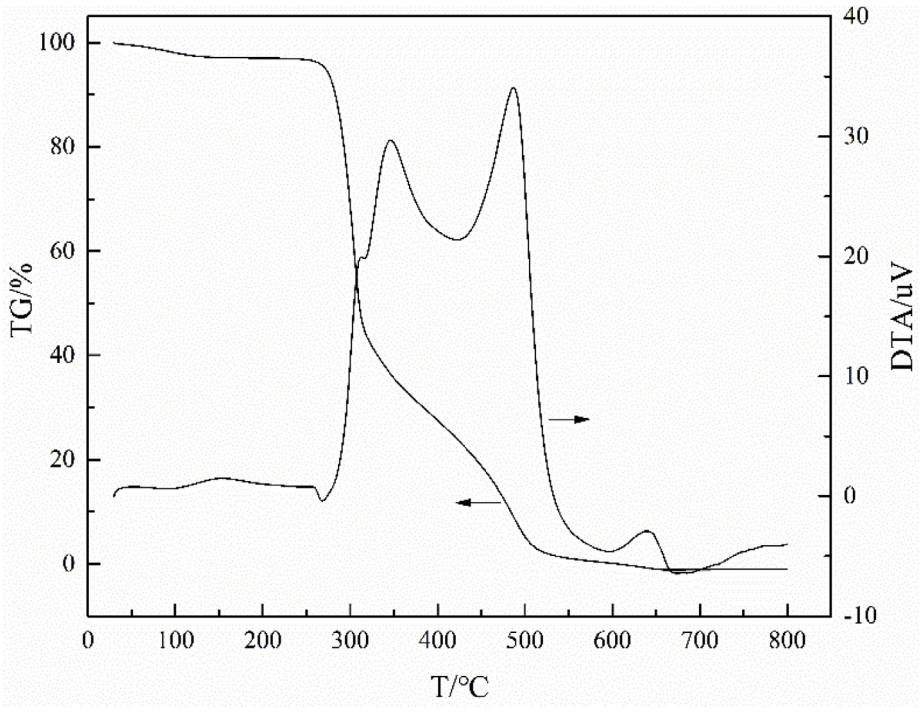

Fig. 9. TG-DTA curve of starch-based sample after drying.

material would inevitably collapse and deform, eventually leading to defects in the ceramic sample after sintering. And no collapse occurred during the formation process. Additionally, the size deviation rate of this slurry after drying was only 1.1%, as shown in Fig. 5. Therefore, based on the above analysis, the starch-based slurry with solid loading of 73.3 wt.% was selected for support structure printing.

Concerning the optimal temperature for burning out the starch slurry, Fig. 9 illustrates the TG-DTA curve of the starch-based sample after drying. Most importantly, the burning away temperature of the support material should not exceed the sintering temperature of the ceramic. As shown in Fig. 9, the left Y-axis shows the relationship between the residual mass of the sample and temperature, while the right Y-axis shows the thermal effect. In spite of the samples being dried in the drying oven before the thermogravimetric analysis, the first weight loss 100 °C was due to the evaporation of water and EtOH. Subsequently, the PVP was decomposed at approximately 300 °C. Thereafter, the mass reduction was due to the burning of the starch. As shown in Fig. 10, when the temperature exceeded 500 °C, the residual mass of the

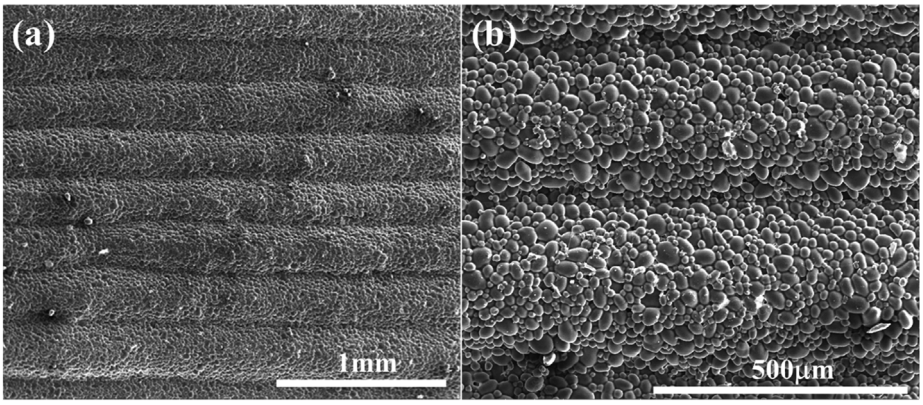

Fig. 10. Diagram of rectangular side wall printed using starch slurry with a solid loading of 73.3 wt.%: (a) side of sample; (b) microscopic morphology between two layers.

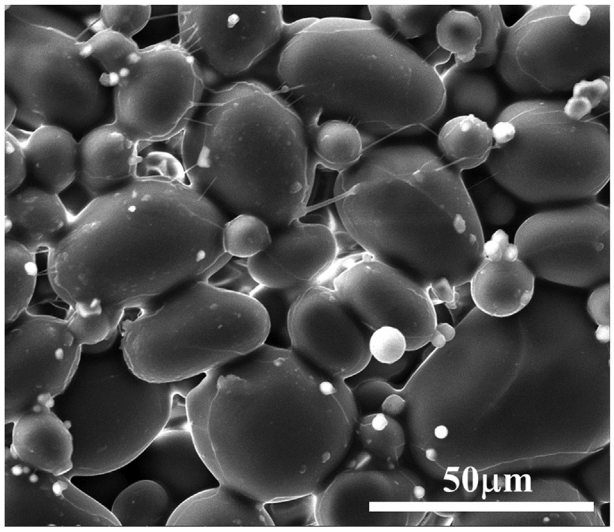

Fig. 11. Microstructure of starch granules after drying.

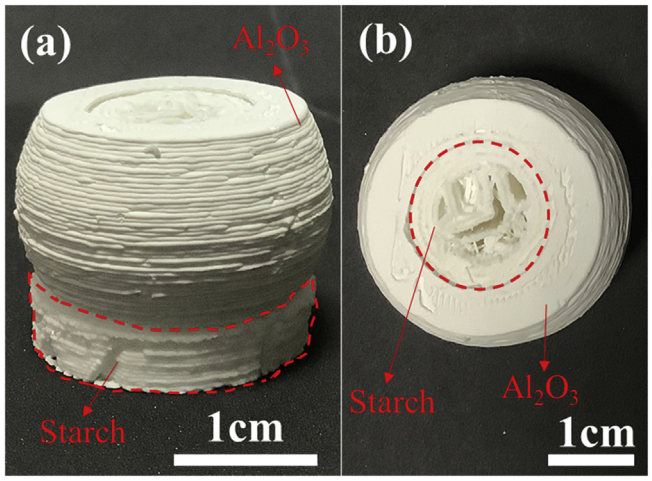

Fig. 12. Al_2O_3 ceramic specimen printed with starch as support material: (a) image from front view and (b) image from top view.

sample was close to 0%, indicating that the sample had been completely decomposed. The reaction of the starch during sintering is shown in Eq. (3):

$$(C_6H_{10}O_5)_n + 6nO_2 \rightarrow 6nCO_2 + 5nH_2O \quad (3)$$

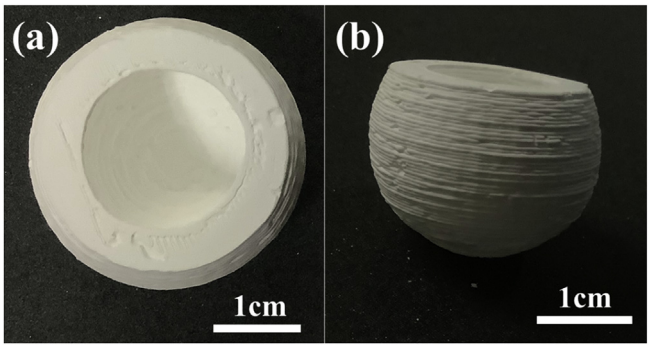

Fig. 13. Al_2O_3 ceramic specimen after sintering: (a) image from top view and (b) image from front view.

The resulting products of the starch are CO_2 and H_2O. The practical sintering temperature of ceramics is generally above 1000 °C, so there will be no residual starch at this temperature.

Additionally, the printing effect of the starch slurry was analyzed. Fig. 10 depicts a diagram of a rectangular side-wall printed using starch slurry with a solid loading of 73.3 wt.%. Evidently, the green bodies prepared from this starch slurry possessed good shape retention, and the layers exhibited a uniform distribution morphology. There was no separation between layers.

Fig. 11 exhibits the microstructure of the starch granules after drying. The starch particles were observed to be spherical and ellipsoidal—as shown in Fig. 11—which improved the fluidity of the starch slurry in the printing process. Moreover, the particles were coated with PVP binder and tightly connected, and there were many bond bridges between the particles, which provides a reasonable interpretation for the bending strength of samples after drying.

To verify the practical feasibility, the optimized starch slurry was used to prepare a support structure for an Al_2O_3 ceramic component; the image of the resulting green body is shown in Fig. 12. Fig. 13 shows the Al_2O_3 ceramic part that was obtained after sintering at 1200 °C for 2 h.

As shown in Fig. 12, there were no cracks in the main and support structure after drying and the interface between the two materials was not separated. The size deviation of the Al_2O_3 and starch samples after drying was relatively small, indicating that the two materials were well-matched. Had there been a large difference in size between the two materials, the ceramic pot may have cracked.

As shown in Fig. 13, all the starch was removed from the sample after sintering at 1200 °C, and the ceramic structure did not deform, crack, or collapse. On this basis, the feasibility of starch as a support material in the preparation of complex ceramic structures has been

demonstrated.

4. Conclusions

(1) A novel starch-based support material including starch, PVP, and anhydrous ethanol was proposed for the preparation of complex ceramic components.
(2) The starch slurries with different solid loadings possessed the rheological properties of shear thinning. When the solid loading was 73.3 wt.%, the size deviation and bending strength of the printed samples after drying were 1.1% and exceeded 11 MPa, respectively.
(3) There was no delamination or cracking between the two materials observed in the Al_2O_3 ceramic part after drying. After sintering at high temperature, the support material was completely removed without residue, and the shape of the main ceramic material was maintained well without deformation or cracking.

Acknowledgements

The authors would like to express their appreciation to the National Natural Science Foundation of China (NSFC) (No.51775204), Innovation Fund of Huazhong University of Science and Technology (NO. 2018JYCXJJ020), State Key Laboratory of Materials Processing and Die and Mould Technology, HUST and the Analytical and Testing Center, HUST.

References

[1] P. Filip, B. Hausnerova, Master flow curves as a tool to modelling ceramic injection molding, Ceram. Int. 45 (2019) 7468–7471.
[2] R.K. Nishihora, P.L. Rachadel, M. Gabriela, N. Quadri, Manufacturing porous ceramic materials by tape casting — a review, J. Eur. Ceram. Soc. 38 (2018) 988–1001.
[3] P. Wiecinska, L. Skrzos, N. Prokurat, New route for processing of multilayer Al_2O_3-Co_3O_4 materials through gelcasting, J. Eur. Ceram. Soc. 37 (2017) 1627–1634.
[4] H. Zhao, C. Ye, Z. Fan, A simple and effective method for gel casting of zirconia green bodies using phenolic resin as a binder, J. Eur. Ceram. Soc. 34 (2014) 1457–1463.
[5] L. Liu, Z. Hou, Y. Zhao, G. Geng, Y. Wang, Fabrication of ZrB_2 ceramics by reactive hot pressing of ZrB and B, J. Am. Ceram. Soc. 101 (2018) 5294–5298.
[6] N. Travitzky, A. Bonet, B. Dermeik, T. Fey, I. Filbert-Demut, L. Schlier, T. Schlordt, P. Greil, Additive manufacturing of ceramic-based materials, Adv. Eng. Mater. 16 (2014) 729–754.
[7] H. Zhao, C. Ye, Z. Fan, C. Wang, 3D printing of CaO-based ceramic core using nanozirconia suspension as a binder, J. Eur. Ceram. Soc. 37 (2017) 5119–5125.
[8] M. Lejeune, T. Chartier, C. Dossou-Yovo, R. Noguera, Ink-jet printing of ceramic micro-pillar arrays, J. Eur. Ceram. Soc. 29 (2009) 905–911.
[9] Z. Pan, Y. Wang, H. Huang, Z. Ling, Y. Dai, S. Ke, Recent development on preparation of ceramic inks in ink-jet printing, Ceram. Int. 41 (2015) 12515–12528.
[10] K. Zhang, R. He, C. Xie, G. Wang, G. Ding, M. Wang, W. Song, D. Fang, Photosensitive ZrO_2 suspensions for stereolithography, Ceram. Int. 45 (2019) 12189–12195.
[11] J.W. Halloran, Ceramic Stereolithography : additive manufacturing for ceramics by photopolymerization, Annu. Rev. Mater. Res. 46 (2016) 10.1–10.22.
[12] G. Zhang, H. Chen, H. Zhou, Additive manufacturing of green ceramic by selective laser gasifying of frozen slurry, J. Eur. Ceram. Soc. 37 (2017) 2679–2684.
[13] C.F. Revelo, H.A. Colorado, 3D printing of kaolinite clay ceramics using the Direct Ink Writing (DIW) technique, Ceram. Int. 44 (2018) 5673–5682.
[14] P. Lima, A. Zocca, W. Acchar, J. Günster, 3D printing of porcelain by layerwise slurry deposition, J. Eur. Ceram. Soc. 38 (2018) 3395–3400.
[15] D. Ortiz-Acosta, T. Moore, D.J. Safarik, K.M. Hubbard, M. Janicke, 3D-Printed silicone materials with hydrogen getter capability, Adv. Funct. Mater. 28 (2018) 1–8.
[16] H.K.A. Renteria-marquez, N.D. Love, Y. Lin, D. Islam, L.A. Chavez, Fabrication of bulk piezoelectric and dielectric $BaTiO_3$ ceramics using paste extrusion 3D printing technique, J. Am. Ceram. Soc. 102 (2019) 3685–3694.
[17] A. Ghazanfari, W. Li, M.C. Leu, G.E. Hilmas, A novel freeform extrusion fabrication process for producing solid ceramic components with uniform layered radiation drying, Addit. Manuf. 15 (2017) 102–112.
[18] Z. Chen, Z. Li, J. Li, C. Liu, C. Lao, Y. Fu, C. Liu, Y. Li, P. Wang, Y. He, 3D printing of ceramics : a review, J. Eur. Ceram. Soc. 39 (2019) 661–687.
[19] S. Tang, Z. Fan, H. Zhao, L. Yang, F. Liu, X. Liu, Layered extrusion forming—a simple and green method for additive manufacturing ceramic core, Int. J. Adv. Manuf. Technol. 96 (2018) 3809–3819.
[20] H. Elsayed, M. Sinico, M. Secco, F. Zorzi, P. Colombo, E. Bernardo, B-doped hardystonite bioceramics from preceramic polymers and fillers: synthesis and application to foams and 3D-printed scaffolds, J. Eur. Ceram. Soc. 37 (2017) 1757–1767.
[21] Y.Y. Li, L.T. Li, B. Li, Direct ink writing of 3-3 piezoelectric composite, J. Alloy. Comp. 620 (2015) 125–128.
[22] Z. Liu, M. Zhang, B. Bhandari, Y. Wang, 3D printing : printing precision and application in food sector, Trends Food Sci. Technol. J. 69 (2017) 83–94.
[23] C. Xu, B. Quinn, L.L. Lebel, D. Therriault, Multi-material direct ink writing (DIW) for complex 3D metallic structures with removable supports, ACS Appl. Mater. Interfaces 11 (2019) 8499–8506.
[24] W. Li, A. Ghazanfari, D. Mcmillen, M.C. Leu, G.E. Hilmas, J. Watts, Fabricating ceramic components with water dissolvable support structures by the Ceramic On-Demand Extrusion process, CIRP Ann. - Manuf. Technol. 66 (2017) 225–228.
[25] L. Yang, S. Tang, G. Li, F. Liu, X. Liu, W. Jiang, Z. Fan, Performance characteristics of collapsible CaO-SiO_2 based ceramic core material via layered extrusion forming, Ceram. Int. 45 (2019) 7681–7689.
[26] F.J. Martínez-vázquez, A. Pajares, P. Miranda, A simple graphite-based support material for robocasting of ceramic parts, J. Eur. Ceram. Soc. 38 (2018) 2247–2250.
[27] Standard test method for flexural strength of advanced ceramics at ambient temperature, ASTM C 1161-02c. ASTM International, West Conshohocken, PA, 2008.
[28] V. De Graef, F. Depypere, M. Minnaert, K. Dewettinck, Chocolate yield stress as measured by oscillatory rheology, Food Res. Int. 44 (2011) 2660–2665.
[29] J.E. Smay, J. Cesarano, J.A. Lewis, Colloidal inks for directed assembly of 3-D periodic structures, Langmuir 18 (2002) 5429–5437.
[30] S. Tang, L. Yang, G. Li, X. Liu, Z. Fan, 3D printing of highly-loaded slurries via layered extrusion forming: parameters optimization and control, Addit. Manuf. 28 (2019) 546–553.
[31] E. Peng, D. Zhang, J. Ding, Ceramic Robocasting : recent achievements , potential , and future developments, Adv. Mater. 1802404 (2018) 1–14.
[32] C.R. Tubío, F. Guitián, A. Gil, Fabrication of ZnO periodic structures by 3D printing, J. Eur. Ceram. Soc. 36 (2016) 3409–3415.
[33] A. Nommeots-Nomm, P.D. Lee, J.R. Jones, Direct ink writing of highly ioactive glasses, J. Eur. Ceram. Soc. 38 (2018) 837–844.